

OpenEarthAgent : A Unified Framework for Tool-Augmented Geospatial Agents

Akashah Shabbir^{1*}, Muhammad Umer Sheikh^{1*}, Muhammad Akhtar Munir¹,
Hiyam Debary², Mustansar Fiaz², Muhammad Zaigham Zaheer¹, Paolo
Fraccaro², Fahad Shahbaz Khan^{1,3}, Muhammad Haris Khan¹, Xiao Xiang
Zhu⁴, and Salman Khan^{1,5}


¹ Mohamed bin Zayed University of Artificial Intelligence

² IBM Research

³ Linköping University

⁴ Technical University Munich

⁵ Australian National University

 <https://github.com/mbzuai-oryx/OpenEarthAgent>

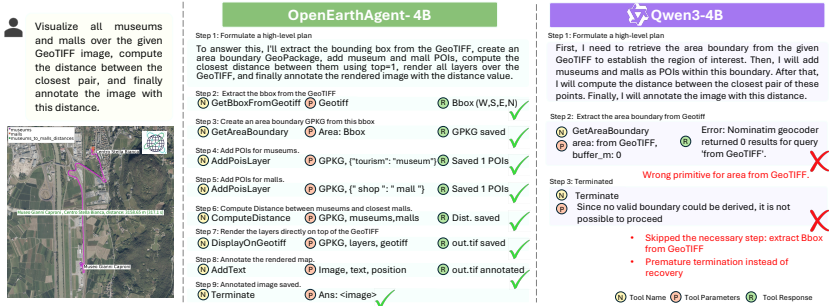


Fig. 1: Comparison between baseline Qwen3-4B and OpenEarthAgent-4B on a GIS reasoning query. OpenEarthAgent executes tools sequentially with correct dependencies and interpretable feedback, while Qwen3 fails due to unordered multi-tool calls and inconsistent reasoning.

Abstract. Recent progress in multimodal reasoning has enabled agents that can interpret imagery, connect it with language, and perform structured analytical tasks. Extending such capabilities to the remote sensing domain remains challenging, as models must reason over spatial scale, geographic structures, and multispectral indices while maintaining coherent multi-step logic. To bridge this gap, OpenEarthAgent introduces a unified framework for developing tool-augmented geospatial agents trained on satellite imagery, natural-language queries, and detailed reasoning traces. The training pipeline relies on supervised fine-tuning over structured reasoning trajectories, aligning the model with verified multi-step tool interactions across diverse analytical contexts. The accompanying corpus comprises 14,538 training and 1,169 evaluation instances, with more than 100K reasoning steps in the training split and over

* Equal contribution.

7K reasoning steps in the evaluation split. It spans urban, environmental, disaster, and infrastructure domains, and incorporates GIS-based operations alongside index analyses such as NDVI, NBR, and NDBI. Grounded in explicit reasoning traces, the learned agent demonstrates structured reasoning, stable spatial understanding, and interpretable behaviour through tool-driven geospatial interactions across diverse conditions. We report consistent improvements over a strong baseline and competitive performance relative to recent open and closed-source models.

1 Introduction

The evolution of visual representation learning has transitioned from static perception to interactive multi-modal reasoning. Early single-shot frameworks such as DINO [3] and MAE [13] laid the foundation for large-scale visual understanding through self-supervised objectives, learning strong image encoders without explicit language-based reasoning or interaction. Inspired by these successes, the remote sensing community extended this paradigm to earth observation, where models such as Prithvi [15], Copernicus-FM [40], Galileo [36], Panopticon [37], TerraFM [6], and AnySat [1] scaled representation learning to global multisensor data. These earth-scale vision models demonstrated remarkable transfer across spatial resolutions and modalities, yet their predictions remained one-shot and perception-centric, focusing on recognition rather than structured reasoning.

In parallel, large multi-modal models have progressed beyond perception. Architectures such as BLIP-2 [18], InstructBLIP [5], LLaVA-OneVision [17], and Kosmos-2 [27] extended language models into the visual domain, enabling grounded image understanding. Building on this trajectory, remote-sensing VLMs emerged to adapt multimodal reasoning to geospatial data. Early efforts such as RemoteCLIP [21], SkySenseGPT [23], and GeoChat [16] introduced large-scale multimodal alignment for remote sensing through paired image-text and instruction-following datasets. Recently, EarthDial [31] advanced this paradigm by extending grounding across optical, SAR, thermal, and temporal modalities, enabling unified multimodal reasoning for classification, captioning, and change analysis. Despite coupling language with perception, current remote sensing VLMs remain largely descriptive and lack explicit structured reasoning.

Subsequent reasoning-centric approaches such as ReAct [47], DeepSeek-R1 [10], and VLM-R1 [30] introduced structured planning and, in some cases, tool-driven reasoning, transforming static perception into organized multi-step task execution. Recent developments such as OpenThinkIMG [33] unified these advances through multi-step vision-tool interaction, where large vision-language models iteratively “*think with images*” through executable reasoning trajectories. Inspired by these advances, efforts such as ThinkGeo [29] and Earth-Agent [7] began exploring tool-augmented reasoning for earth observation (EO). They demonstrate that large models can plan analytical chains but still face challenges in geospatial grounding, coordinate consistency, and physically verifiable

outputs. These limitations highlight the need for geographically grounded agents that integrate perception with explicit and interpretable reasoning.

Building on this motivation, we construct a comprehensive agentic corpus and training framework that integrates GIS-based layers, index-driven computations, and multisensor imagery, including both optical and SAR modalities, to support a wide spectrum of EO reasoning tasks. Our dataset comprises training image-query reasoning-trace instances, along with a held-out evaluation set designed to benchmark model consistency and reasoning performance across diverse geospatial scenes. The data span diverse contexts, including urban infrastructure, environmental monitoring, disaster assessment, land-use mapping, and transportation analysis, and incorporate GIS operations (e.g., distance, area, zonal statistics) alongside index-based analyses such as NDVI, NBR, and NDBI. Each sample provides an explicit reasoning trajectory linking multiple tool calls, intermediate states, and outcomes, enabling agents to learn structured, interpretable workflows rather than static predictions.

To assess generalization and reasoning fidelity, we benchmark a broad suite of large and reasoning models, including the GPT family [25], Qwen [46], InternLM [2], and other recent multimodal LLMs. Our dataset is constructed through a unified data-gathering pipeline, where each modality undergoes question synthesis and automated validation to ensure reasoning diversity, spatial grounding, and cross-source consistency. This large-scale, tool-augmented corpus bridges the divide between GIS analysis and remote-sensing perception, providing a unified setting for evaluating structured geospatial reasoning. This work introduces an agentic framework for remote sensing that integrates tool-based reasoning within a unified training and evaluation setup.

Specifically, our key contributions are:

- **Unified data-construction pipeline:** A systematic process integrating multisensor imagery (RGB, SAR), GIS layers, and index-based computations through question synthesis and automated validation.
- **Structured reasoning-alignment framework:** A supervised training setup that aligns multi-step tool interactions to ensure consistent reasoning flow and spatially grounded decision making (Fig. 1).
- **Comprehensive multimodal corpus:** 14,538 training instances and 1,169 evaluation tasks establishing a benchmark for studying spatial reasoning, grounding, and interpretability across reasoning and non-reasoning models.

2 Related Work

Remote sensing has progressed from task-specific models to large-scale foundation and vision-language models trained on global, multimodal data. Early self-supervised methods [4, 24] established transferable pretraining strategies on Sentinel archives. Subsequent foundation models include Prithvi-v2 [35] with spatiotemporal transformers on HLS, Copernicus-FM [40] with metadata-aware hypernetworks for Sentinel, Panopticon [37] and AnySat [1] with spectral- and

resolution-adaptive embeddings, and CROMA [8] fusing radar and optical contrastive learning. Galileo [36] captures global-to-local context, demonstrating scalable pretraining across diverse sensors and geographies. On the multimodal side, GeoChat [16] enabled language grounding to satellite imagery, and EarthDial [31] extended this paradigm to multi-resolution optical, SAR, thermal, and temporal modalities across diverse tasks. Despite their scalability and representational strength, these models remain largely single-pass encoders; they lack structured reasoning, tool orchestration, and verifiable intermediate analysis.

Alongside foundation models, agentic systems have emerged that couple reasoning with external tools and feedback-driven control. Early frameworks such as ReAct [47] and Voyager [39] demonstrated the transition from static inference to autonomous, goal-directed reasoning. Subsequent systems, including WebAgent [42], VisTA [14], and DeepEyes [50], introduced modular architectures capable of selecting and sequencing tools under guided supervision, improving reasoning depth and execution consistency. OpenThinkIMG [33] unified these ideas through large-scale visual-tool integration with standardized APIs, while OctoTools [22] emphasized modular, verifiable execution via structured tool interfaces. Collectively, these systems established key principles: looped reasoning, standardized tool I/O, and trajectory-based learning, yet remain geospatially naive, lacking coordinate awareness, scale handling, and domain-specific spatial verification essential for earth observation analysis.

An emerging wave of EO research is now bringing these agentic principles into geospatial contexts. ThinkGeo [29] frames EO question answering as tool-augmented reasoning, benchmarking ReAct-style chains and exposing persistent weaknesses in coordinate consistency, spatial grounding, and multi-step planning. Earth-Agent [7] broadens the tool ecosystem to include spectral products and standardized interfaces but still relies on largely predefined workflows, limiting physically verifiable GIS and index-based reasoning. Geo-OLM [32] explores plan-tool-verify prompting for compact models, improving efficiency but depending primarily on prompt-level heuristics rather than learned adaptive policies. Building on this gap, we introduce an EO-native agentic stack that unifies dataset construction, supervised reasoning alignment, and evaluation under a physically grounded framework. OpenEarthAgent enables broad orchestration of GIS, index-based, optical, and SAR operations through structured instruction-tool pairs; trains on detailed reasoning traces with a dedicated evaluation set; and supports interpretable, verifiable, multi-step reasoning across diverse geospatial conditions.

3 Dataset Curation

We curate a large-scale remote-sensing dataset linking imagery, queries, and tool-based reasoning traces to enable interpretable, multi-step geospatial analysis.

Overview and Motivation: The dataset presented in this work serves as a foundation for training and evaluating tool-augmented geospatial reasoning agents. While recent EO datasets primarily focus on visual classification or re-

Method	RS	MM	MS	GIS	Spec	CD	RData
ReAct [47]	✗	✗	✓	✗	✗	✗	✗
OpenThinkIMG [33]	✗	✗	✓	✗	✗	✗	✓
ThinkGeo [29]	✓	✓	✓	✗	✗	✓	✗
Earth-Agent [7]	✓	✓	✓	✓	✓	✗	✗
Geo-OLM [32]	✓	✗	✓	✗	✗	✗	✗
RS-Agent [45]	✓	✗	✗	✗	✗	✗	✗
RS-ChatGPT [11]	✓	✗	✗	✗	✗	✗	✗
OpenEarthAgent (Ours)	✓	✓	✓	✓	✓	✓	✓

Table 1: Comparison of geospatial/EO agent frameworks. Abbrev.: RS=remote sensing; MM=multimodal inputs; Tools=executable tool/function calls; MS=multi-step reasoning; GIS=GIS/vector-raster geospatial; Spec=spectral (e.g., indices, multi-spectral); CD=change detection; RData=reasoning-supervision data for training.

trieval, they lack explicit reasoning structure and tool-level traceability. Our dataset bridges this gap by integrating imagery, natural-language queries, reasoning traces, and tool executions in a unified schema. It aims to teach models not only to recognize patterns in satellite data but also to plan, verify, and compute through structured analytical workflows. A comparative overview against existing agent frameworks is provided in Table 1, highlighting differences in modality coverage, tool integration, reasoning depth, and supervision design. In total, it contains 14,538 training samples and 1,169 held-out test samples for benchmarking, covering diverse geographic regions, sensor modalities, and reasoning tasks designed for interpretable multi-step learning and evaluation.

Data Sources and Composition: The dataset integrates heterogeneous imagery and metadata from open-access EO repositories, encompassing optical, SAR, GIS, and multispectral domains. Primary sources include high-resolution benchmarks such as DOTA [43], DIOR [19], xBD [12], AID [44], NWPU-VHR-10 [38], FloodNet [28], and Global-Dumpsite [34], complemented by Sentinel collections and Google Earth Engine archives (see Table ?? for details). Each dataset offers distinct spatial resolutions and annotation formats (bounding boxes, segmentation masks, category labels), providing both fine-grained object understanding and large-scale semantic context. The collection spans seven thematic domains: *urban planning, disaster assessment, environmental monitoring, transportation, aviation, recreation, and industrial infrastructure*. Multispectral and indexed layers (e.g., NDVI, NBR, NDBI) are derived through Google Earth Engine to complement optical and SAR imagery with physically meaningful environmental indicators. Where required for spatial reasoning tasks, samples are associated with geospatial metadata such as coordinates, projection reference, and ground sampling distance (GSD), enabling verifiable geospatial analysis.

Automated Curation Pipeline and Quality Control: Dataset construction begins by aggregating candidate regions, annotations, and metadata from multiple geospatial sources. For RGB-SAR branches, a *Sample Sufficiency Filter* module removes datapoints that do not meet the required annotation counts, after which an *Annotation Harmonizer* module aligns labels across source datasets

Source	Annotation Type	Sensor (m/px)	Year	Applications / Tasks
OPTICAL DATASETS				
DIOR [19]	B-Box, Category	0.5–30	2024	Transport & Aviation Monitoring; Infrastructure Mapping
DOTA [43]	GSD, B-Box, Category	0.1–1	2021	Transport Surveillance; Infrastructure Assessment
NWPU-VHR-10 [38]	B-Box, Category	0.5–2	2023	Aviation; Transport; Infrastructure
UCAS-AOD [51]	B-Box, Category	0.5–2	2015	Aviation; Transport
AID [44]	B-Box, Category	0.2–2	2017	Urban Planning; Industrial Site Detection
iSAID [41]	GSD, B-Box, Seg. Map, Pix. Count	0.1–1	2019	Segmentation; Transport Monitoring
xBD [12]	GSD, B-Box, Category, Pix. Count	1–3.5	2019	Disaster Assessment; Change Detection
FloodNet [28]	GSD, B-Box, Category, Seg. Map, Pix. Count	0.015–0.02	2020	Flood Monitoring; Damage Estimation
Global-Dumpsite [34]	B-Box, Category	0.3–0.8	2023	Environmental Monitoring; Waste Localization
SAR DATASETS				
SSDD [49]	B-Box, Category	1–15	2021	Ship Detection; Maritime Transport
SADD [48]	B-Box, Category	0.5–3	2022	Aviation; Vessel Identification
SIVED [20]	B-Box, Category	0.1–0.3	2023	Vehicle Detection; Transport Monitoring
GIS-BASED SOURCES				
OpenStreetMap [26]	POIs (Points of Interest)	N/A	2017–	Urban Mapping; Infrastructure Analysis
INDEXED / MULTISPECTRAL SOURCES				
Google Earth Engine [9]	Index Layers	10–30	2017–	Urban Planning; Change Detection; Environmental Monitoring

Table 2: Comprehensive overview of data sources used for dataset construction, covering optical, SAR, GIS, and multispectral domains. These sources collectively offer complementary spatial resolutions, and annotation formats, ranging from urban and transport monitoring to environmental and disaster assessment, forming a rich foundation for multi-sensor, tool-based geospatial reasoning. GSD = ground sample distance, B-Box = bounding box, Seg. = segmentation.

to produce a unified annotation format. Index-based samples are mined by detecting temporal variations in spectral indicators such as vegetation loss, burn severity, or flooding. All sources are converted into a unified JSON schema encapsulating imagery paths, GeoPackage metadata, spatial attributes, and tool arguments. Before the final generation, candidate GIS queries are programmatically executed (e.g., POI counting, distance computation, area estimation) to verify argument correctness and prevent formatting inconsistencies. Potential inconsistencies such as mismatches between query instructions and tool parameters or invalid execution outputs are automatically detected, followed by controlled regeneration and targeted manual verification when necessary.

Natural-language queries and corresponding reasoning trajectories are synthesized through a structured LLM-driven module. We curate prompt templates per task type and employ one-shot exemplars tailored to each reasoning cate-

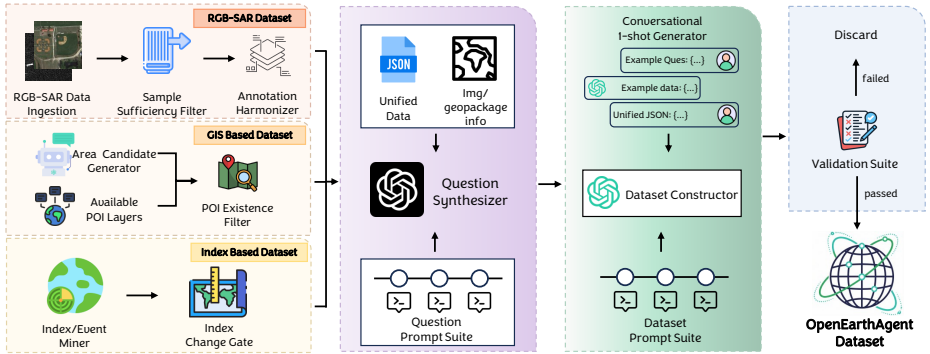


Fig. 2: Unified data-curation pipeline for OpenEarthAgent Dataset. The process integrates diverse data sources: RGB-SAR imagery, GIS-based spatial layers, and index-driven datasets to build a harmonized geospatial corpus. Each branch performs its own filtering: RGB-SAR samples undergo sufficiency and annotation checks; GIS scenes are selected using point-of-interest (POI) constraints; and index-based inputs capture spectral changes (e.g., NDVI, NBR, NDBI). The outputs are merged into unified JSON records containing imagery metadata and geopackage information. A question synthesizer and conversational one-shot generator create tool-grounded queries and reasoning traces, which are validated through an automated suite ensuring geographic and syntactic correctness. Invalid instances are discarded, while verified ones form the final high-quality corpus used for agentic training and evaluation.

gory. Once finalized, the data generator produces complete entries that contain queries, multimodal inputs, and serialized reasoning traces. Each instance is validated by executing the corresponding tool calls to verify argument correctness, geometric validity, and spatial consistency. All test-set samples additionally pass manual inspection to ensure realistic geospatial measurements (e.g., correcting GSD inconsistencies that may produce unrealistic area estimates). Validated samples are incorporated into the final corpus. A summary of the pipeline is shown in Fig. 2.

Task Structure and Query Design: Each instance represents a query-driven reasoning process that transforms static observation into an iterative perception-action loop (see Fig. 3). Queries are expressed in natural language and paired with structured reasoning traces that interleave *thoughts*, *actions*, and *observations*, ultimately converging on a final *answer*. These traces span diverse modalities and task types, including: GIS operations (distance, buffer, area, zonal statistics), object-level reasoning (counting, comparison, orientation, proximity), spectral index computation (NDVI, NBR, NDBI), and temporal change detection. Reasoning depth and tool sequence length vary across samples, but each trajectory provides a complete chain of intermediate steps, enabling transparent multi-step geospatial problem solving rather than one-shot prediction.

Dataset Statistics: Fig. 4 summarizes the scale and structure of the OpenEarthAgent dataset. The training split contains 14,538 instances and the benchmark split contains 1,169 evaluation samples. Each instance includes multimodal

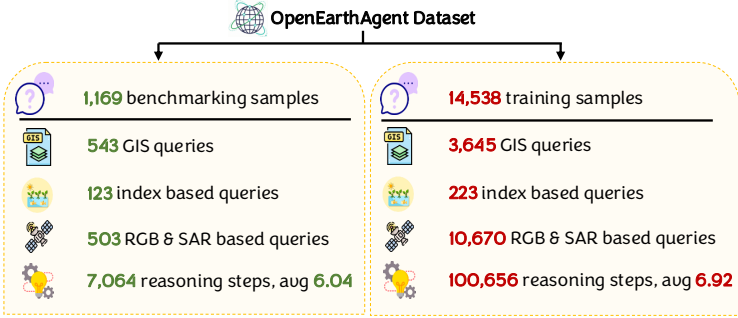
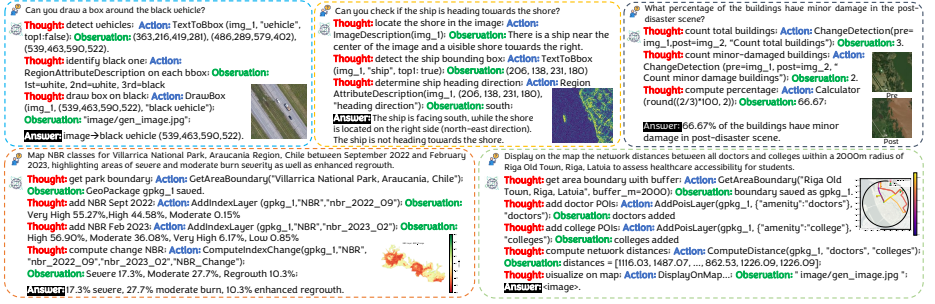


Fig. 4: Key statistics for the curated corpus used for training and evaluation of our proposed agentic pipeline.

imagery, a natural-language query, and a structured reasoning trace with interleaved tool calls and intermediate observations. Across the training set, the corpus contains 100,656 reasoning steps (average 6.92 per query) and the benchmark split contains 7,064 reasoning steps (average 6.04 per query). Reasoning steps correspond to explicit thought-action-observation transitions, while tool calls capture the diversity of operational pathways required for solving curated agentic tasks. The breadth of modalities, thematic coverage, and depth of reasoning traces enable rigorous evaluation of grounded, interpretable, and tool-augmented geospatial reasoning.

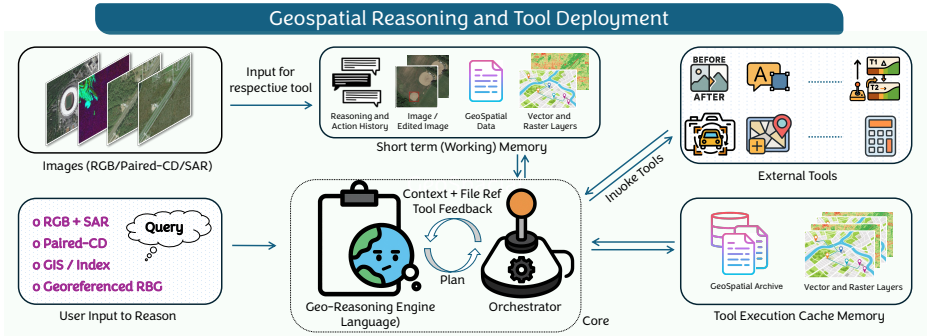


Fig. 5: Overview of the proposed *OpenEarthAgent* framework. The figure depicts tool deployment, where user queries over RGB, SAR, paired change-detection (CD), or GIS/indexed imagery are processed by the geospatial reasoning engine and tool orchestrator, which invoke appropriate tools and integrate feedback.

4 Methodology

4.1 Overview

We present *OpenEarthAgent*, a unified agentic learning framework designed for multimodal reasoning over earth observation data. The framework integrates tool-driven interaction and language-grounded reasoning into a single end-to-end formulation. Unlike conventional multimodal models that process all inputs in one step, *OpenEarthAgent* decomposes geospatial reasoning into an organized sequence of perception and action steps, where the agent learns to *perceive*, *reason*, and *act* through callable tools operating on visual, textual, and spatial modalities. Given a natural-language instruction \mathbf{u} and corresponding multimodal inputs \mathbf{v} (e.g., RGB imagery, paired change-detection inputs, SAR, GIS layers, or georeferenced raster data), the agent generates multi-step reasoning trajectories that interleave internal thoughts with explicit tool invocations and their returned outputs (see Fig. 5). At each step, the agent maintains a short-term working memory that contains: instruction, observations, prior tool calls, spatial metadata, and contextual feedback from previous executions. This working memory enables iterative reasoning and consistent spatial grounding. Training follows a supervised fine-tuning procedure on validated reasoning traces, improving syntactic validity, spatial consistency, and multi-step reasoning coherence across diverse geospatial contexts.

4.2 Unified Tool Registry

To standardize the diverse operators used in EO reasoning, we construct a unified tool registry that abstracts heterogeneous visual, spectral, and GIS operations through a consistent callable schema:

$$\mathcal{M}_j = (\mathbf{x}_{\text{in}}, \mathbf{y}_{\text{out}}, \psi_j), \quad (1)$$

where \mathbf{x}_{in} denotes structured input arguments, \mathbf{y}_{out} denotes structured outputs, $\psi_j : \mathbf{x}_{\text{in}} \mapsto \mathbf{y}_{\text{out}}$ is the executable function implementing the operation. All tools follow standardized JSON-based contracts to ensure consistent serialization and validation across training and inference. A central orchestrator parses model-generated tool calls, validates arguments, executes ψ_j , and appends returned outputs to the working memory. During execution, a predicted tool invocation s_t with arguments $\hat{\mathbf{x}}_t$ is evaluated as $\mathbf{y}_t = \psi_{s_t}(\hat{\mathbf{x}}_t)$, and the returned output \mathbf{y}_t becomes part of the updated reasoning context.

To ensure efficiency and consistency, intermediate outputs (e.g., derived vector layers, raster subsets, index maps, computed geometries) are stored in a tool execution cache memory. This cache includes geospatial archives and vector/raster layers that can be reused by subsequent tool calls within the same trajectory. Caching prevents redundant computation and ensures deterministic replay of reasoning steps. New tools can be integrated by registering their schema \mathcal{M}_j without retraining the backbone model, ensuring extensibility while maintaining interface consistency. We outline the tool categories below.

a) Perceptual Tools. These operators form the perceptual layer of the agent, grounding language into image-space entities. Functions such as `TextToBbox`, `ObjectDetection`, and `RegionAttributeDescription` convert free-form queries into spatial primitives such as bounding boxes and semantic tags. `CountGivenObject` and `SegmentObjectPixels` extend these capabilities toward quantitative perception and support object counting and pixel-level area estimation. `ChangeDetection` bridges spatial and temporal understanding by analyzing multi-date pairs to detect semantic or structural changes such as damage or flooding.

b) GIS Computation Tools. To enable explicit geographic reasoning, the registry includes tools for geometric and coordinate-aware computation. Operators such as `GetAreaBoundary`, `AddPoisLayer`, and `ComputeDistance` manipulate vector geometries within standard coordinate reference systems. Outputs include numerical measures (e.g., distances, buffers, zonal statistics) or derived layers that can be visualized via `DisplayOnMap`. These tools support verifiable geodesic reasoning and metric-scale analysis.

c) Spectral Tools. A subset of operators performs band arithmetic and spectral analysis using raster inputs. `AddIndexLayer`, `ComputeIndexChange`, and `ShowIndexLayer` compute and visualize vegetation, burn, or built-up indices (e.g., NDVI, NBR, NDBI). These tools expose physically meaningful variables and enable quantitative reasoning over environmental dynamics.

d) Georeferenced Raster Tools. Tools such as `GetBboxFromGeotiff` and `DisplayOnGeotiff` operate directly on georeferenced raster data. They allow coordinate extraction, bounding box derivation, and visualization aligned with spatial metadata. These operators ensure spatial consistency when reasoning over projected raster datasets.

e) Utility Tools. Generic reasoning utilities such as `Calculator`, `Solver`, and `Plot` support arithmetic computation and symbolic reasoning. Visualization aids like `DrawBox` and `AddText` render intermediate reasoning results. OCR and

GoogleSearch extend multimodal understanding through text extraction and contextual retrieval. **Terminate** signals completion of a reasoning trajectory.

4.3 Reasoning Trajectories and Training Objective

Each training sample encodes a structured reasoning trajectory that connects an instruction \mathbf{u} , observations \mathbf{v} , and a sequence of tool interactions. Formally, the trajectory is represented as:

$$\begin{aligned}\Gamma_i &= \{(s_t, r_t)\}_{t=1}^{T_i}, \quad s_t \in \mathcal{S}, \\ r_t &\sim \mathcal{E}(s_t \mid \mathbf{u}_i, \mathbf{v}_i, \{(s_k, r_k)\}_{k < t}),\end{aligned}\quad (2)$$

where \mathcal{S} denotes the set of registered tools, \mathcal{E} denotes the execution environment (tool controller + cache), and (s_t, r_t) is the t -th action-result pair. Each s_t corresponds to a predicted tool invocation, while r_t is the structured observation returned by the environment.

The autoregressive model conditions on the full working memory state when predicting the next action. Training is performed via maximum likelihood estimation over verified trajectories, optimizing only the tool-action policy:

$$\mathcal{L}_{\text{train}} = -\frac{1}{N} \sum_{i=1}^N \sum_{t=1}^{T_i} \log P_{\eta}(s_t \mid \mathbf{u}_i, \mathbf{v}_i, s_{<t}, r_{<t}), \quad (3)$$

where η parameterizes the model and N is the number of training samples. Tool observations r_t are appended to the working memory as contextual inputs but are masked from loss computation and not treated as policy outputs. This formulation enforces syntactic validity of tool calls, argument correctness, sequential consistency, and spatial coherence while preserving the environment-policy separation.

Before inclusion in training, each trajectory undergoes deterministic replay through the tool controller. Re-execution verifies argument formatting, coordinate integrity, geometric validity, and full-chain executability. Through supervised fine-tuning on validated multi-step trajectories, OpenEarthAgent learns to generate syntactically correct, spatially grounded, and interpretable reasoning workflows over heterogeneous EO data.

5 Experiments

In this section, we outline implementation details, describe the step-by-step and end-to-end evaluation modes, and define metrics used to quantify reasoning fidelity, tool effectiveness, and geospatial accuracy.

5.1 Implementation Details

OpenEarthAgent is finetuned using Qwen3-4B-Instruct-2507 as the base model. Training was performed on LLM controller on four NVIDIA A100 GPUs (40

GB). The base model is loaded via Unsloth’s FastLanguageModel, enabling efficient multi-GPU distributed training. The model is trained for one epoch with a learning rate of 2×10^{-5} , cosine learning rate scheduling, 0.05 warmup ratio, and a batch size of 16. The maximum sequence length is set to 4096 tokens to support long-context conversational tool interactions.

LLM is finetuned on conventional data, where the model alternates between text generation and tool invocation, providing tool outputs and feedback in JSON format, embedded in its user and assistant turns. Training applies response-only masking, computing loss exclusively on assistant-generated tokens, enabling accurate tool calls and structured responses without optimizing on prompt text or external tool outputs. This enables the model to establish a good grounding for tool invocation.

5.2 Baseline Evaluation

To evaluate OpenEarthAgent, we benchmark its performance against a diverse set of large language models (LLMs), encompassing both proprietary and open-source variants. The comparison includes advanced frontier models (GPT-4o and its reasoning-optimized variant o4-mini), and mid- to small-scale open-weight models, including Llama3.1 and Internlm3. All models serve as interchangeable backbones within the unified OpenEarthAgent framework. We assess performance using both step-by-step and end-to-end protocols, allowing analysis of intermediate reasoning trajectories and final task completion accuracy.

Step-by-Step Evaluation: This mode measures procedural reasoning and tool-invocation behavior without executing tools. The model is given n reasoning steps and must generate a valid action at each one based on the full interaction history. The first step is exempt from validation to allow the model to formulate an initial high-level plan before committing to concrete tool interactions. This setup isolates reasoning quality and enables focused analysis of spatial semantics, plan coherence, and geospatial context understanding.

End-to-End Evaluation: This mode tests full autonomous execution with live tool use. The model issues tool calls, forms arguments, and reasons step-by-step based on prior outputs. This setting captures operational robustness, error handling, and how well the model links perception with action in geospatial workflows.

Evaluation Metrics: We assess the model’s procedural reasoning with five metrics. Instance Accuracy (Inst.) measures the proportion of tool called without logical or syntactic errors; Tool Accuracy (Tool) evaluates correctness of tool selection; Argument Name Accuracy (ArgN) checks the presence of all required arguments in the generated action; Argument Value Accuracy (ArgV) verifies argument correctness; and Summarization Accuracy (SummAcc) quantifies how well the model consolidates information from prior tool calls into a coherent final response. We compute F_1 for tool selection across four functional categories: Perception (Per.), Operation (Op.), Logic (Logic.), and GIS (GIS.) to capture alignment between predicted and reference tool sets. Trajectory quality is further assessed via tool-order accuracy under increasing constraints: *Unique*

Model	Param.	Inst.	Tool.	ArgN.	ArgV.	Summ.
FRONTIERLLMs						
gpt-4o		99.18	93.88	85.48	45.80	86.76
o4-mini		83.68	68.33	64.17	37.95	89.48
OPEN-SOURCELLMs						
Qwen2.5-Instruct	7B	94.08	85.51	78.46	38.00	80.08
Llama-3.1-Instruct	8B	47.07	39.30	34.11	17.49	79.08
Internlm3-Instruct	8B	44.54	38.46	27.82	13.25	29.84
Mistralv0.3-Instruct	7B	64.14	35.12	26.11	12.45	24.04
Qwen2.5-Instruct	3B	85.07	72.13	64.87	24.12	68.75
BASELINELLM						
Qwen3-Instruct-2507	4B	97.34	86.94	84.12	33.55	83.28
OPENEARTHAGENT						
OpenEarthAgent	4B	99.51	97.18	96.08	62.10	83.64

Table 3: Step-by-step evaluation under tool-agnostic rollouts. We report accuracies: Inst.; syntactic + logical validity of actions, Tool.; correct tool selection, ArgN.; presence of required parameters, ArgV.; parameter correctness, and Summ.; correctness of the final consolidated answer. While frontier LLMs lead on summary accuracy, OpenEarthAgent attains state-of-the-art Inst./Tool./ArgN./ArgV., narrowing the gap despite a substantially smaller parameter budget.

checks tool-to-tool correspondence without penalizing repeated calls, *AnyOrder* requires all tools (including duplicates) regardless of order, and *SameOrder* enforces both correct sequence and frequency of tool invocations. Overall task Accuracy compares final model completions with reference outputs. For image-generation tasks, success is determined by the correctness of generation tool calls and their execution success rate; all non-generation queries are evaluated by an LLM judge (gpt-4o-mini) using a standardized elaboration evaluation prompt.

5.3 Results

In step-by-step evaluation (Table 3), frontier models lead, with o4-mini scoring highest on Summ. (89.48) and gpt4o showing strong Inst./Tool. accuracy. Among open-source models, Qwen2.5-Instruct (7B) performs competitively (Inst. 94.08, Tool. 85.51), whereas other 7B–8B models show notable degradation, particularly on argument value prediction. OpenEarthAgent (4B) substantially narrows this gap despite its smaller size, achieving state-of-the-art Inst./ Tool./ ArgN./ and ArgV.(99.51/97.18/96.08/62.10) while substantially improving answer accuracy (45.26). In end-to-end evaluation (Table 4), GPT-4o excels on Op. F₁ (66.91) but shows modest Per./Logic. Conversely, OpenEarthAgent delivers balanced gains across Per./Op./Logic./GIS and dominates in tool-order accuracy (AnyOrder/SameOrder/Unique \approx 67-72%), indicating robust trajectory planning rather than isolated tool correctness. Overall, these results suggest that targeted training with tool schemas and trajectories can outperform larger gen-

eral models on geospatial tool-use, especially under strict order/frequency constraints.

Model	Param.	F1 scores				Tool Order			Accuracy	
		Per.	Op.	Logic.	GIS.	AnyOr.	SameO.	Uni.	Ans.	Gen.
FRONTIERLLMS										
gpt-4o		44.47	66.91	35.95	95.80	50.81	50.38	55.52	39.22	77.93
o4-mini		39.48	64.93	12.38	86.51	40.12	39.95	41.49	35.18	55.17
OPEN-SOURCELLMS										
Qwen2.5-Instruct	7B	20.38	37.33	26.68	75.46	31.57	30.02	36.61	15.85	41.38
Llama-3.1-Instruct	8B	22.54	16.45	32.03	64.64	39.01	37.72	44.91	12.70	55.17
Internlm3-instruct	8B	5.50	14.21	0.51	31.47	2.22	1.88	3.16	0.24	2.76
Mistral-Instruct-v0.3	7B	6.74	10.24	15.82	17.12	2.65	2.57	2.91	0.39	5.52
Qwen2.5-Instruct	3B	15.63	16.54	11.16	35.64	9.24	8.72	12.40	1.83	24.14
BASELINELLM										
Qwen3-Instruct-2507	4B	13.86	20.95	18.35	71.82	16.00	14.71	21.47	13.72	15.86
OPENEARTHAGENT										
OpenEarthAgent	4B	58.30	56.76	51.18	98.52	67.75	67.24	72.71	45.26	75.86

Table 4: End-to-end evaluation: (i) F₁ scores for tool selection by functional category: Perception (Per.), Operation (Op.), Logic (Logic.), and GIS (GIS); computed against the reference tool sets; (ii) tool-order fidelity: *AnyOrder* (multiset match, order-agnostic), *SameOrder* (exact sequence match), and *Unique* (set match ignoring multiplicity); and (iii) task-level Accuracy, *Ans.* for non-generative completions and *Gen.* for image-generation success. GPT-4o shows very high GIS F₁, while OpenEarthAgent achieves strong, balanced performance and markedly superior trajectory fidelity, indicating robust multi-step planning rather than isolated tool correctness.

Tool Call & Success Patterns: Proprietary models (gpt-4o, o4-mini) show strong tool-control, issuing thousands of calls with low error rates ($\sim 7\%$), indicating stable formatting and reasoning. OpenEarthAgent executes a higher volume of tool calls while achieving a superior overall success rate. In contrast, open-source models such as Qwen2.5-7B, Qwen2.5-3B, and Llama-3.1-8B exhibit high failure rates (43-46%), reflecting weak adherence to the tool schema. Mistral-7B demonstrates a lower error rate but fails to invoke tools at the required adequacy to meet task demands. Despite extensive tool usage, Llama-3.1-8B and Mistral-7B fail to converge to a final answer within the allowed step, resulting in 94% and 98% incomplete task executions, respectively. Overall, performance as shown in Fig. 6 varies by call volume and precision: robust models maintain low error rates, while others struggle with consistent, well-formed tool invocations.

Category Scores: As seen in Fig. 7, OpenEarthAgent (79.43%) and gpt4o (79.39%) achieve the strongest index-based scores, substantially outperforming all baselines. GIS-based tasks reveal a sharper degradation, with OpenEarthAgent (55.77 %) followed by gpt4o (41.95 %) and o4mini (39.55%). Open-source models such as qwen2-5-7b, qwen3-4b, and llama3.1-8b perform comparably well on image-based queries, while smaller models approach zero on index tasks and score only marginally on GIS and image-based tasks. Overall, the results high-

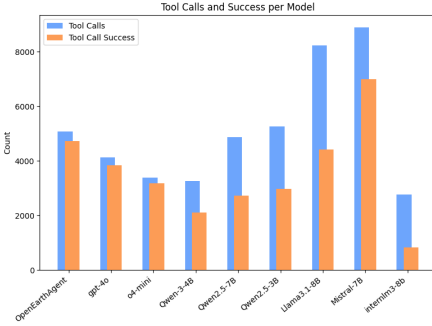


Fig. 6: Comparison of model tool-call performance: Open-source models show lower success rates, while GPT-4o and OpenEarthAgent achieve significantly more successful calls.

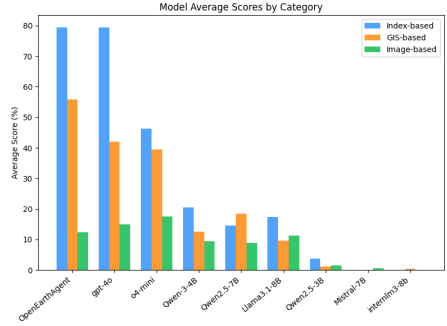


Fig. 7: Category-wise performance: OpenEarthAgent and o4mini lead in index-/GIS-based scores while some open source perform comparably on image-based queries.

light a significant performance gap and show that index- and GIS-based reasoning remains particularly difficult for smaller open models.

6 Conclusion

We introduced *OpenEarthAgent*, a unified framework for tool-augmented geospatial reasoning that connects natural language with multimodal earth observation data through structured analytical workflows. Unlike conventional EO models that focus solely on perception, OpenEarthAgent performs grounded, interpretable reasoning by orchestrating visual, spectral, GIS, and GeoTIFF-aware tools under a consistent executable schema. The accompanying corpus comprises 14,538 training instances and 1,169 held-out test instances, each containing validated multi-step reasoning trajectories with explicit tool calls, intermediate observations, and outputs. OpenEarthAgent addresses a fundamental gap in the EO community: the absence of advanced benchmarks and training frameworks that move from perception-only modeling toward structured, verifiable geospatial reasoning. We believe this work offers a valuable step toward agentic AI systems for environmental monitoring, disaster response, infrastructure analysis, and broader geospatial decision-making applications.

References

1. Astruc, G., Gonthier, N., Mallet, C., Landrieu, L.: Anysat: One earth observation model for many resolutions, scales, and modalities. In: Proceedings of the Computer Vision and Pattern Recognition Conference. pp. 19530–19540 (2025)
2. Cai, Z., Cao, M., Chen, H., Chen, K., Chen, K., Chen, X., Chen, X., Chen, Z., Chen, Z., Chu, P., Dong, X., Duan, H., Fan, Q., Fei, Z., Gao, Y., Ge, J., Gu, C.,

- Gu, Y., Gui, T., Guo, A., Guo, Q., He, C., Hu, Y., Huang, T., Jiang, T., Jiao, P., Jin, Z., Lei, Z., Li, J., Li, J., Li, L., Li, S., Li, W., Li, Y., Liu, H., Liu, J., Hong, J., Liu, K., Liu, K., Liu, X., Lv, C., Lv, H., Lv, K., Ma, L., Ma, R., Ma, Z., Ning, W., Ouyang, L., Qiu, J., Qu, Y., Shang, F., Shao, Y., Song, D., Song, Z., Sui, Z., Sun, P., Sun, Y., Tang, H., Wang, B., Wang, G., Wang, J., Wang, J., Wang, R., Wang, Y., Wang, Z., Wei, X., Weng, Q., Wu, F., Xiong, Y., Xu, C., Xu, R., Yan, H., Yan, Y., Yang, X., Ye, H., Ying, H., Yu, J., Yu, J., Zang, Y., Zhang, C., Zhang, L., Zhang, P., Zhang, P., Zhang, R., Zhang, S., Zhang, S., Zhang, W., Zhang, W., Zhang, X., Zhang, X., Zhao, H., Zhao, Q., Zhao, X., Zhou, F., Zhou, Z., Zhuo, J., Zou, Y., Qiu, X., Qiao, Y., Lin, D.: Internlm2 technical report (2024)
3. Caron, M., Touvron, H., Misra, I., Jégou, H., Mairal, J., Bojanowski, P., Joulin, A.: Emerging properties in self-supervised vision transformers. In: Proceedings of the IEEE/CVF international conference on computer vision. pp. 9650–9660 (2021)
 4. Cong, Y., Khanna, S., Meng, C., Liu, P., Rozi, E., He, Y., Burke, M., Lobell, D., Ermon, S.: Satmae: Pre-training transformers for temporal and multi-spectral satellite imagery. *Advances in Neural Information Processing Systems* **35**, 197–211 (2022)
 5. Dai, W., Li, J., Li, D., Tiong, A., Zhao, J., Wang, W., Li, B., Fung, P.N., Hoi, S.: Instructblip: Towards general-purpose vision-language models with instruction tuning. *Advances in neural information processing systems* **36**, 49250–49267 (2023)
 6. Danish, M.S., Munir, M.A., Shah, S.R.A., Khan, M.H., Anwer, R.M., Laaksonen, J., Khan, F.S., Khan, S.: Terrafrm: A scalable foundation model for unified multi-sensor earth observation. *arXiv preprint arXiv:2506.06281* (2025)
 7. Feng, P., Lv, Z., Ye, J., Wang, X., Huo, X., Yu, J., Xu, W., Zhang, W., Bai, L., He, C., et al.: Earth-agent: Unlocking the full landscape of earth observation with agents. *arXiv preprint arXiv:2509.23141* (2025)
 8. Fuller, A., Millard, K., Green, J.: Croma: Remote sensing representations with contrastive radar-optical masked autoencoders. *Advances in Neural Information Processing Systems* **36**, 5506–5538 (2023)
 9. Google Earth Engine: Google earth engine. <https://earthengine.google.com/> (2025)
 10. Guo, D., Yang, D., Zhang, H., Song, J., Wang, P., Zhu, Q., Xu, R., Zhang, R., Ma, S., Bi, X., et al.: Deepseek-r1 incentivizes reasoning in llms through reinforcement learning. *Nature* **645**(8081), 633–638 (2025)
 11. Guo, H., Su, X., Wu, C., Du, B., Zhang, L., Li, D.: Remote sensing chatgpt: Solving remote sensing tasks with chatgpt and visual models. In: *IGARSS 2024-2024 IEEE International Geoscience and Remote Sensing Symposium*. pp. 11474–11478. IEEE (2024)
 12. Gupta, R., Hosfelt, R., Sajeew, S., Patel, N., Goodman, B., Doshi, J., Heim, E., Choset, H., Gaston, M.: xbd: A dataset for assessing building damage from satellite imagery. *arXiv preprint arXiv:1911.09296* (2019)
 13. He, K., Chen, X., Xie, S., Li, Y., Dollár, P., Girshick, R.: Masked autoencoders are scalable vision learners. In: *Proceedings of the IEEE/CVF conference on computer vision and pattern recognition*. pp. 16000–16009 (2022)
 14. Huang, Z., Ji, Y., Rajan, A.S., Cai, Z., Xiao, W., Wang, H., Hu, J., Lee, Y.J.: Visualtoolagent (vista): A reinforcement learning framework for visual tool selection. *arXiv preprint arXiv:2505.20289* (2025)
 15. Jakubik, J., Roy, S., Phillips, C., Fraccaro, P., Godwin, D., Zadrozny, B., Szwarcman, D., Gomes, C., Nyirjesy, G., Edwards, B., et al.: Foundation models for generalist geospatial artificial intelligence. *arXiv preprint arXiv:2310.18660* (2023)

16. Kuckreja, K., Danish, M.S., Naseer, M., Das, A., Khan, S., Khan, F.S.: Geochat: Grounded large vision-language model for remote sensing. In: Proceedings of the IEEE/CVF Conference on Computer Vision and Pattern Recognition. pp. 27831–27840 (2024)
17. Li, B., Zhang, Y., Guo, D., Zhang, R., Li, F., Zhang, H., Zhang, K., Zhang, P., Li, Y., Liu, Z., et al.: Llava-onevision: Easy visual task transfer. arXiv preprint arXiv:2408.03326 (2024)
18. Li, J., Li, D., Savarese, S., Hoi, S.: Blip-2: Bootstrapping language-image pre-training with frozen image encoders and large language models. In: International conference on machine learning. pp. 19730–19742. PMLR (2023)
19. Li, K., Wan, G., Cheng, G., Meng, L., Han, J.: Object detection in optical remote sensing images: A survey and a new benchmark. ISPRS journal of photogrammetry and remote sensing **159**, 296–307 (2020)
20. Lin, X., Zhang, B., Wu, F., Wang, C., Yang, Y., Chen, H.: Sived: A sar image dataset for vehicle detection based on rotatable bounding box. Remote Sensing **15**(11), 2825 (2023)
21. Liu, F., Chen, D., Guan, Z., Zhou, X., Zhu, J., Ye, Q., Fu, L., Zhou, J.: Remoteclip: A vision language foundation model for remote sensing. IEEE Transactions on Geoscience and Remote Sensing **62**, 1–16 (2024)
22. Lu, P., Chen, B., Liu, S., Thapa, R., Boen, J., Zou, J.: Octotools: An agentic framework with extensible tools for complex reasoning. arXiv preprint arXiv:2502.11271 (2025)
23. Luo, J., Pang, Z., Zhang, Y., Wang, T., Wang, L., Dang, B., Lao, J., Wang, J., Chen, J., Tan, Y., et al.: Skysensegpt: A fine-grained instruction tuning dataset and model for remote sensing vision-language understanding. arXiv preprint arXiv:2406.10100 (2024)
24. Manas, O., Lacoste, A., Giró-i Nieto, X., Vazquez, D., Rodriguez, P.: Seasonal contrast: Unsupervised pre-training from uncured remote sensing data. In: Proceedings of the IEEE/CVF International Conference on Computer Vision. pp. 9414–9423 (2021)
25. OpenAI: Introducing gpt. <https://openai.com> (2025)
26. OpenStreetMap contributors: Openstreetmap: Collaborative project to create a free editable map of the world. <https://www.openstreetmap.org> (2025)
27. Peng, Z., Wang, W., Dong, L., Hao, Y., Huang, S., Ma, S., Wei, F.: Kosmos-2: Grounding multimodal large language models to the world. arXiv preprint arXiv:2306.14824 (2023)
28. Rahnemounfar, M., Chowdhury, T., Sarkar, A., Varshney, D., Yari, M., Murphy, R.R.: Floodnet: A high resolution aerial imagery dataset for post flood scene understanding. IEEE Access **9**, 89644–89654 (2021)
29. Shabbir, A., Munir, M.A., Dudhane, A., Sheikh, M.U., Khan, M.H., Fraccaro, P., Moreno, J.B., Khan, F.S., Khan, S.: Thinkgeo: Evaluating tool-augmented agents for remote sensing tasks. arXiv preprint arXiv:2505.23752 (2025)
30. Shen, H., Liu, P., Li, J., Fang, C., Ma, Y., Liao, J., Shen, Q., Zhang, Z., Zhao, K., Zhang, Q., et al.: Vlm-r1: A stable and generalizable r1-style large vision-language model. arXiv preprint arXiv:2504.07615 (2025)
31. Soni, S., Dudhane, A., Debary, H., Fiaz, M., Munir, M.A., Danish, M.S., Fraccaro, P., Watson, C.D., Klein, L.J., Khan, F.S., et al.: Earthdial: Turning multi-sensory earth observations to interactive dialogues. In: Proceedings of the Computer Vision and Pattern Recognition Conference. pp. 14303–14313 (2025)

32. Stamoulis, D., Marculescu, D.: Geo-olm: Enabling sustainable earth observation studies with cost-efficient open language models & state-driven workflows. In: *Proceedings of the ACM SIGCAS/SIGCHI Conference on Computing and Sustainable Societies*. pp. 608–619 (2025)
33. Su, Z., Li, L., Song, M., Hao, Y., Yang, Z., Zhang, J., Chen, G., Gu, J., Li, J., Qu, X., et al.: Openthinking: Learning to think with images via visual tool reinforcement learning. *arXiv preprint arXiv:2505.08617* (2025)
34. Sun, X., Yin, D., Qin, F., Yu, H., Lu, W., Yao, F., He, Q., Huang, X., Yan, Z., Wang, P., et al.: Revealing influencing factors on global waste distribution via deep-learning based dumpsite detection from satellite imagery. *Nature Communications* **14**(1), 1444 (2023)
35. Szwarcman, D., Roy, S., Fraccaro, P., Gíslason, P.E., Blumenstiel, B., Ghosal, R., de Oliveira, P.H., Almeida, J.L.d.S., Sedona, R., Kang, Y., et al.: Prithvi-eo-2.0: A versatile multi-temporal foundation model for earth observation applications. *arXiv preprint arXiv:2412.02732* (2024)
36. Tseng, G., Fuller, A., Reil, M., Herzog, H., Beukema, P., Bastani, F., Green, J.R., Shelhamer, E., Kerner, H., Rolnick, D.: Galileo: Learning global and local features in pretrained remote sensing models. *arXiv e-prints* pp. arXiv–2502 (2025)
37. Waldmann, L., Shah, A., Wang, Y., Lehmann, N., Stewart, A., Xiong, Z., Zhu, X.X., Bauer, S., Chuang, J.: Panopticon: Advancing any-sensor foundation models for earth observation. In: *Proceedings of the Computer Vision and Pattern Recognition Conference*. pp. 2204–2214 (2025)
38. Wang, C., Bai, X., Wang, S., Zhou, J., Ren, P.: Multiscale visual attention networks for object detection in vhr remote sensing images. *IEEE Geoscience and Remote Sensing Letters* **16**(2), 310–314 (2018)
39. Wang, G., Xie, Y., Jiang, Y., Mandlekar, A., Xiao, C., Zhu, Y., Fan, L., Anandkumar, A.: Voyager: An open-ended embodied agent with large language models. *arXiv preprint arXiv:2305.16291* (2023)
40. Wang, Y., Xiong, Z., Liu, C., Stewart, A.J., Dujardin, T., Bountos, N.I., Zavras, A., Gerken, F., Papoutsis, I., Leal-Taixé, L., et al.: Towards a unified copernicus foundation model for earth vision. *arXiv preprint arXiv:2503.11849* (2025)
41. Waqas Zamir, S., Arora, A., Gupta, A., Khan, S., Sun, G., Shahbaz Khan, F., Zhu, F., Shao, L., Xia, G.S., Bai, X.: isaid: A large-scale dataset for instance segmentation in aerial images. In: *Proceedings of the IEEE/CVF conference on computer vision and pattern recognition workshops*. pp. 28–37 (2019)
42. Wei, Z., Yao, W., Liu, Y., Zhang, W., Lu, Q., Qiu, L., Yu, C., Xu, P., Zhang, C., Yin, B., et al.: Webagent-r1: Training web agents via end-to-end multi-turn reinforcement learning. *arXiv preprint arXiv:2505.16421* (2025)
43. Xia, G.S., Bai, X., Ding, J., Zhu, Z., Belongie, S., Luo, J., Datcu, M., Pelillo, M., Zhang, L.: Dota: A large-scale dataset for object detection in aerial images. In: *Proceedings of the IEEE conference on computer vision and pattern recognition*. pp. 3974–3983 (2018)
44. Xia, G.S., Hu, J., Hu, F., Shi, B., Bai, X., Zhong, Y., Zhang, L., Lu, X.: Aid: A benchmark data set for performance evaluation of aerial scene classification. *IEEE Transactions on Geoscience and Remote Sensing* **55**(7), 3965–3981 (2017)
45. Xu, W., Yu, Z., Mu, B., Wei, Z., Zhang, Y., Li, G., Peng, M.: Rs-agent: automating remote sensing tasks through intelligent agent. *arXiv preprint arXiv:2406.07089* (2024)
46. Yang, A., Li, A., Yang, B., Zhang, B., Hui, B., Zheng, B., Yu, B., Gao, C., Huang, C., Lv, C., et al.: Qwen3 technical report. *arXiv preprint arXiv:2505.09388* (2025)

47. Yao, S., Zhao, J., Yu, D., Du, N., Shafran, I., Narasimhan, K.R., Cao, Y.: React: Synergizing reasoning and acting in language models. In: The eleventh international conference on learning representations (2022)
48. Zhang, P., Xu, H., Tian, T., Gao, P., Li, L., Zhao, T., Zhang, N., Tian, J.: Sepnet: Scale expansion and feature enhancement pyramid network for sar aircraft detection with small sample dataset. *IEEE Journal of Selected Topics in Applied Earth Observations and Remote Sensing* **15**, 3365–3375 (2022)
49. Zhang, T., Zhang, X., Li, J., Xu, X., Wang, B., Zhan, X., Xu, Y., Ke, X., Zeng, T., Su, H., et al.: Sar ship detection dataset (ssdd): Official release and comprehensive data analysis. *Remote Sensing* **13**(18), 3690 (2021)
50. Zheng, Z., Yang, M., Hong, J., Zhao, C., Xu, G., Yang, L., Shen, C., Yu, X.: Deepeyes: Incentivizing "thinking with images" via reinforcement learning. arXiv preprint arXiv:2505.14362 (2025)
51. Zhu, H., Chen, X., Dai, W., Fu, K., Ye, Q., Jiao, J.: Orientation robust object detection in aerial images using deep convolutional neural network. In: 2015 IEEE international conference on image processing (ICIP). pp. 3735–3739. IEEE (2015)

Supplementary

OpenEarthAgent: A Unified Framework for Tool-Augmented Geospatial Agents

This supplementary material includes quantitative results illustrating multiple evaluation cases (S1). It also provides a model selection criterion(S2), error analysis (S3), a detailed overview of input-output structures with corresponding tool descriptions (S4), and an evaluation prompt(S5).



Fig. A1: Example illustrates the zero-shot geospatial reasoning capabilities of OpenEarthAgent on a real-world environmental task by generating a Normalized Burn Ratio (NBR) difference map for a given region. The NBR difference map shows pronounced negative values (red) in southern Topanga, revealing burn scars and vegetation loss, while northern areas remain stable (yellow), showing the post-fire effects from early 2025 events.

S1 Qualitative Results

Figure A1 presents a zero-shot example demonstrating the geospatial reasoning capability of OpenEarthAgent. Given a natural language instruction, the agent autonomously composes a complete multi-step workflow. The agent first formulates a plan to extract the park boundary, compute NBR layers, evaluate their difference, and visualize the result. It sequentially invokes the tools `GetAreaBoundary`, `AddIndexLayer` (for December 2024 and February 2025), `ComputeIndexChange`, and `ShowIndexLayer`, generating a differenced NBR (dNBR) layer that quantifies vegetation loss and recovery. The reasoning trace(middle) of Figure A1 illustrates coherent tool grounding and correct argument formatting across the entire chain.

Figure A2 illustrates an example of OPENEARTHAGENT performing metric-scale geospatial reasoning. Given a natural-language query about the distance

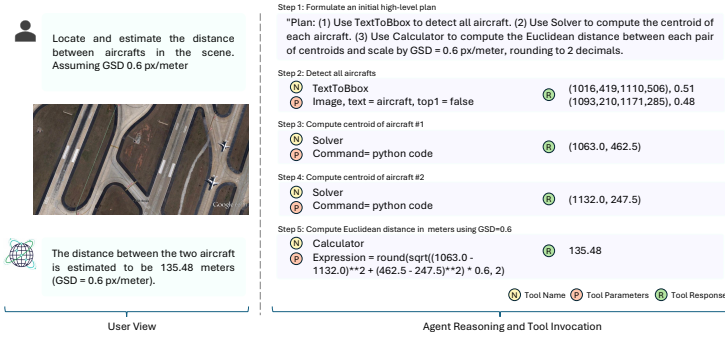


Fig. A2: Example demonstrating OPENEARTHAGENT’s capability for metric-scale geospatial reasoning from imagery, estimating an airplane-to-airplane distance using centroid detection and GSD scaling.

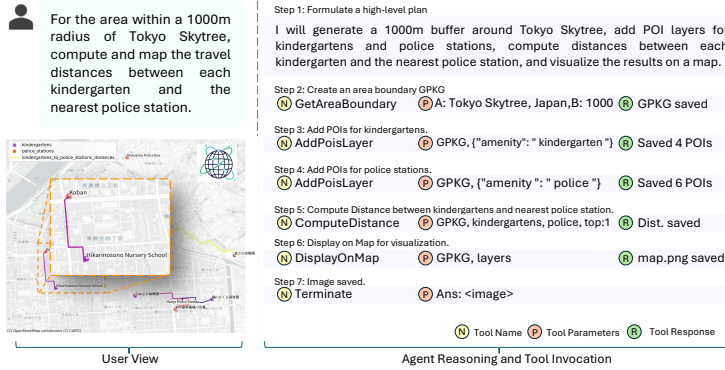


Fig. A3: Example demonstrating OPENEARTHAGENT’s road-network distance computation and spatial analysis within a 1000 m buffer of a specified area. The visualization highlights the detailed map output generated through sequential tool orchestration.

between two vehicles with a GSD of 0.072, the agent composes a workflow: detecting vehicles via **TextToBbox**, computing centroids with **Solver**, and calculating Euclidean distance using **Calculator**. The reasoning trace shows coherent tool use and precise cross-modal computation. In Figure A3 the agent extracts the buffered area, adds POI layers, computes nearest-neighbor road distances from each kindergarten to the closest police station, and visualizes the POIs and distance links on a base map. This demonstrates the agent’s ability to integrate spatial query and interpretable visualization within a unified reasoning pipeline.

S2 Model Selection

To determine how underlying model capacity affects tool-use accuracy and multi-step reasoning, we compare two model backbones trained under identical data,

Base Model	F ₁ scores				Tool Order			Accuracy	
	Per.	Op.	Logic.	GIS.	AnyO.	SameO.	Unique	Ans.	Gen.
OPENEARTHAGENT									
Qwen2.5-7B-Instruct	96.72	97.41	88.60	99.53	74.80	74.80	96.00	23.19	89.67
Qwen3-4B-Instruct-2507	97.82	97.70	91.39	99.53	81.80	81.60	97.50	23.47	90.76

Table A1: Comparison of base model performance across reasoning and tool-usage metrics. Qwen3-4B-Instruct-2507 slightly outperforms Qwen2.5-7B-Instruct. Results highlight that improved architectural alignment in the Qwen3 series yields more efficient multi-step reasoning despite a smaller model size.

hyperparameter, and tool-conditioning settings: Qwen3-4B-Instruct-2507 and Qwen2.5-7B-Instruct. We train on 25% of the training corpus and reserve an internal 8% split from it as a held-out validation set used only for model selection, entirely separate from the benchmark test set.

As summarized in Table A1, the smaller Qwen3-4B-Instruct-2507 outperforms the 7B counterpart across nearly all metrics, particularly in logical reasoning (Logic F₁: +2.79) and tool-order consistency (AnyO: +7.0). This indicates that architectural refinements and improved alignment in the Qwen3 series enhance structured reasoning efficiency even with fewer parameters. Both variants exhibit near-saturated GIS and operational F₁ scores, confirming that tool-augmented reasoning generalizes robustly across these domains. The marginal differences in answer and generation accuracy further suggest that reasoning quality is independent of model scale. Overall, Qwen3-4B-Instruct-2507 delivers a superior balance between model size and reasoning reliability, making it a strong candidate for a baseline model for scalable geospatial applications.

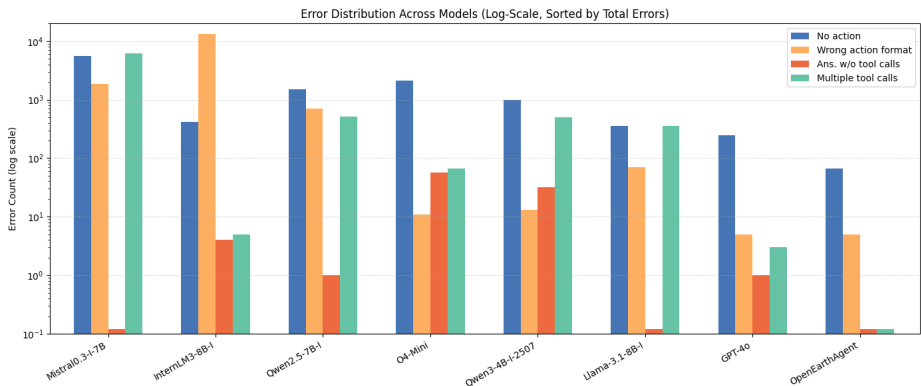


Fig. A4: Log-scale error distribution across models for four error types: No action, Wrong action format, Answer reached without a single tool call, and Multiple tool calls in a single action. Frontier models show fewer errors overall, while the fine-tuned OpenEarthAgent achieves the lowest total error count.

S3 Error Analysis

We conduct a fine-grained analysis of model failures to better understand where tool-augmented reasoning breaks down. Figure A4 shows errors across 4 types, and reports their frequency across some evaluated models.

Syntax errors occur when the model fails to comply with the prescribed output syntax, such as missing required actions(No Action) or producing malformed JSON structures(Wrong action format). Each conversation allows a single “thought-only” turn for initial planning, but all subsequent turns are expected to include at least one valid action. Open-source models exhibit notably higher rates of such violations, particularly **Mistral0.3-7B-Instruct** and **InternLM3-8B-Instruct**, which frequently omit or incorrectly format tool calls. In contrast, **GPT-4o** shows substantially fewer syntax-related failures, indicating stronger adherence to structured output specifications. **OPENEARTHAGENT** exhibits the fewest syntax errors overall, suggesting that fine-tuned tool schema conditioning substantially improves output validity.

The reasoning errors are failures in multi-step logic and tool selection, including queries that reach an answer without a single tool call (Ans. w/o tool call) and redundant tool calls in a single step (Multiple tool calls). “Answer w/o tool call” errors are rare across models, showing that most models correctly trigger tools when needed, except **Qwen3-4B-Instruct-2507** and **o4-mini**, which omit calls more often. Conversely, “Multiple tool calls” are more prevalent, particularly in **Mistral0.3-7B-Instruct**, indicating over-generation and weaker action control. Frontier model (**GPT-4o**) maintains tighter regulation, while **OPENEARTHAGENT** achieves the best balance, invoking tools only when required and avoiding both omissions and redundancies.

S4 Tools I/O Structure

The tools used in OpenEarthAgent span a wide range of perceptual, geometric, and analytical operations. They include basic utilities such as drawing boxes, adding text, OCR, and solvers, etc., alongside higher-level tools for object detection, region description, change detection, and pixel-level segmentation. GIS functions such as retrieving area boundaries, adding POI layers, and computing distances, etc., provide the spatial backbone needed for grounded reasoning. Spectral tools further extend this capability by generating and comparing index layers such as NDVI or NDBI. Each tool follows a clear schema with defined inputs and outputs (see Table A2), allowing the agent to compose them into transparent, multi-step reasoning chains across imagery, metadata, and geospatial layers.

S5 Evaluation Prompt

To evaluate the geospatial agent’s outputs, we adopt a structured Answer Accuracy assessment framework, illustrated in Fig. A5. The evaluation protocol

measures the alignment between a model’s predicted answer and the corresponding ground truth using a normalized score $[0,1]$. The framework distinguishes between numerical and non-numerical outputs. Quantitative responses are evaluated using a $\pm 10\%$ tolerance threshold, whereas spatial outputs use Intersection over Union (IoU) thresholds. For descriptive or categorical answers, evaluation is based on semantic equivalence, considering paraphrasing, partial correctness, and contradictions. The protocol further defines strict handling of missing, fabricated, or non-responsive outputs, assigning zero scores where required elements are absent or invalid. To standardize assessment, the framework enforces a constrained JSON output format consisting of a numerical score and a concise justification.

You are an evaluation assistant responsible for measuring the Answer Accuracy Score (a value between 0 and 1) for a geospatial agent's prediction. You are given:

- A Question
- A Ground Truth Answer
- A Predicted Answer produced by the agent

Your task is to evaluate how accurately the Predicted Answer matches the Ground Truth Answer, considering both numerical precision and semantic correctness. When numerical values are present, allow a $\pm 10\%$ tolerance range for acceptable variation. For descriptive or categorical outputs, judge based on meaningful semantic equivalence.

Evaluation Guidelines

1. Numerical or Quantitative Comparisons

- A predicted numeric value is correct if it lies within $\pm 10\%$ of the corresponding value in the ground truth.
- For bounding boxes, consider the prediction correct if the IoU (Intersection over Union) ≥ 0.5 .
- If multiple numeric values exist:
 - Compute element-wise difference.
 - All values within $\pm 10\%$ range \rightarrow Score = 0.95 - 1.00 (highly accurate)
 - Most values within $\pm 10\%$ range \rightarrow Score = 0.80 - 0.94 (minor acceptable deviations)
 - Some values within $\pm 10\%$ range \rightarrow Score = 0.30 - 0.79 (partially correct)
 - Most values within $\pm 20\%$ range \rightarrow Score = 0.10 - 0.29 (partially aligned)
 - All values incorrect or nonsensical \rightarrow Score = 0.00 (completely incorrect)
- Ignore extraneous numbers that do not directly answer the question.

2. Non-Numerical or Categorical Comparisons

- Evaluate semantic equivalence:
 - Perfect semantic match \rightarrow Score = 1.0
 - Minor phrasing or synonym difference \rightarrow 0.8-0.9
 - Partially correct (missing non-critical details) \rightarrow 0.4-0.8
 - Vague or weakly related \rightarrow 0.1-0.4
 - Contradictory or incorrect \rightarrow 0.0

3. Handling Missing or Contradictory Content

- If the prediction omits all required answer elements \rightarrow Score = 0.0
- If the prediction introduces fabricated entities, relationships, or placeholders \rightarrow Score = 0.00
- If a numeric answer is required and the model responds with "no data", "unknown", or similar \rightarrow Score = 0.00

You must provide your evaluation strictly in the following format and nothing else:

```
{
  "Score": <float between 0.0 and 1.0>,
  "Justification": "<1-2 concise sentences explaining the score based on the comparison between
  GT and Pred>"
}
```

Fig. A5: Evaluation Prompt for Geospatial Agent Answer Accuracy Assessment. The figure shows the structured prompt used to compute an Answer Accuracy Score (0–1) for a geospatial agent's prediction. It defines criteria for numerical tolerance, semantic equivalence, error handling, and required JSON output format for standardized evaluation.

Table A2: List of available tools with brief descriptions, inputs, and outputs.

Tool Name	Description	Input	Output
Calculator	Evaluates math expressions using Python.	Math expression (Python syntax)	Numeric result as text
OCR	Extract text from an image.	Image	Text with bounding boxes
DrawBox	Draws a box on an image.	Image, box coords, optional label	Image with drawn box
AddText	Adds text to an image.	Image, text, position, optional color	Image with text overlay
GoogleSearch	Returns search results from Google.	Query string, optional number of results	Search result text
Plot	Plots data using Python code.	Python code defining <code>solution()</code>	Generated plot image
Solver	Solves equations using sympy.	Python code defining <code>solution()</code> and using sympy	Equation solution as string
TextToBbox	Finds object based on description.	Image, object description	Bounding box coordinates
ImageDescription	Generates caption for image.	Image	Text description
RegionAttribute-Description	Describes attribute in region or image.	Image, attribute, optional bbox	Text description of attribute
CountGivenObject	Counts objects in an image.	Image, object name, optional bbox	Integer count
ChangeDetection	Describes changes between two images.	Text query, pre and post images	Description of changes
SegmentObject-Pixels	Segments objects and counts pixels.	Image, object name, optional flag	Pixel count(s)
ObjectDetection	Detects objects in the image.	Image	Labels, boxes, scores
GetAreaBoundary	Gets area boundary as GeoPackage.	Place name or bbox, optional buffer	GeoPackage with boundary
AddPoisLayer	Adds POIs to GeoPackage.	GeoPackage, query, layer name	Confirmation with POI count
ComputeDistance	Computes distance between layers.	GeoPackage, source and target layers	Summary text and layer name
DisplayOnMap	Renders the map image from layers.	GeoPackage, layer names	PNG image path
AddIndexLayer	Computes spectral index layer.	GeoPackage, index type, year, name	Saved layer and class stats
ComputeIndex-Change	Computes change between index layers.	GeoPackage, index type, layer names	Saved change layer and stats
ShowIndexLayer	Generates a preview of the raster index.	GeoPackage, index type, layer name	Preview image path
GetBboxFrom-Geotiff	Extract an area bounding box (W, S, E, N) from a GeoTIFF	GeoTiff	GeoPackage with boundary
DisplayOnGeotiff	Render GeoPackage layers (with feature names) over a given GeoTIFF	GeoPackage, layers, GeoTiff	rendered GeoTiff
Terminate	Ends task and returns final answer.	Final answer text	None